공학석사학위논문

분극곡선과 전기화학 임피던스 분광법을 통한 고분자 전해질 연료전지 저항 분리에 대한 연구

Resistance Separation of Polymer Electrolyte Membrane Fuel Cell by Polarization Curve and Electrochemical Impedance Spectroscopy

2019 년 8 월

서울대학교 대학원

기계항공공학부

최 재 현

분극곡선과 전기화학 임피던스 분광법을 통한 고분자 전해질 연료전지 저항 분리에 대한 연구

Resistance Separation of Polymer Electrolyte Membrane Fuel Cell by Polarization Curve and Electrochemical Impedance Spectroscopy

지도교수 민 경 덕

이 논문을 공학석사 학위논문으로 제출함

2019 년 4 월

서울대학교 대학원

기계항공공학부

최 재 현

최재현의 공학석사 학위논문을 인준함

2019 년 6 월

위 원 장 _____

부위원장 _____

위 원 _____

Abstract

Resistance Separation of Polymer Electrolyte Membrane Fuel Cell by Polarization Curve and Electrochemical Impedance Spectroscopy

Jaehyeon Choi

Department of Mechanical and Aerospace Engineering

The Graduate School

Seoul National University

The separation of resistance is a main issue to improve the performance of a polymer electrolyte membrane (PEM) fuel cell. To separate the resistance, electrochemical impedance spectroscopy (EIS) and polarization curve are the major methodologies. In addition, to analyze the EIS, an equivalent circuit is selected; therefore, it is also a major issue. Although it has been an object of study for a long time; less attention has been given to separate the resistance, including the protonic resistance in the cathode catalyst layer (CCL). In this study, to separate the total resistance, a new method using the polarization curve and EIS was suggested for various operating conditions. Then, the overpotential was estimated to investigate the effect of each resistance.

First, a general solution was derived using the recursion formula to fit the Nyquist plot of the EIS. Second, to separate the total resistance, a polarization curve and EIS with an approximated solution were used. The error of the total resistance from the approximated solution at a RH 80 and 100% were around 1.5 and 1%, respectively. In addition, each resistance from the polarization curve was well matched with the EIS results ($R^2 > 0.995$ and RMSE < 0.01).

Protonic resistance in the CCL was significantly changed by the water content. To fully consider the relationship between diffusion and the effective protonic resistance in the CCL, these experiments were carried out in the Heliox condition. As the effective diffusion coefficient increased, the effective protonic resistance in the CCL decreased under high current density region due to the migration of the reaction points. The overpotential by the charge transfer resistance had the largest contribution (46.5 ~ 86.9%), and the overpotential by the ohmic resistance linearly increased with the current density. This study can help to identify the effect of the resistance in terms of the voltage and to improve the performance of PEM fuel cells.

Keywords: Resistance separation, Overpotential, Electrochemical impedance spectroscopy (EIS), Polarization curve, Protonic resistance, Water content

Student Number: 2017-22150

Contents

List of Figures

List of Tables

Nomenclature

r_p	distributed protonic resistance in the CCL, Ω cm
r_{ct}	distributed charge transfer resistance, Ω cm
z_W	distributed BCPE, Ω cm
r_{mass}	distributed mass transport resistance, Ω cm
q_C	parameter related to CPE, Ω^{-1} cm^{-3} s^{P_C}
P_C	CPE exponent
q_B	distributed parameter related to BCPE, Ω^{-1} cm^{-3} s^{P_B}
P_B	BCPE exponent
k	iteration number of the node, $1 \leq k \leq n-1$
n	total repeating number of the node
HFR	high frequency resistance, Ω cm^2
R_p	protonic resistance in the CCL, Ω cm^2
R_p^{eff}	effective protonic resistance in the CCL, Ω cm^2
R_{ct}	charge transfer resistance, Ω cm^2
Z_W	BCPE, Ω cm^2

R_{mass}	mass transfer resistance, $\Omega\ \mathrm{cm}^2$
R_{ohmic}	ohmic resistance, $\Omega\ \mathrm{cm}^2$
R_{total}	total resistance, $\Omega\ \mathrm{cm}^2$
Q_C	parameter related to CPE, $\Omega^{-1}\ \mathrm{cm}^{-2}\ \mathrm{s}^{P_C}$
Q_B	parameter related to BCPE, $\Omega^{-1}\ \mathrm{cm}^{-2}\ \mathrm{s}^{P_B}$
D^{eff}	effective diffusion coefficient of oxygen diffusion in the CCL, $\mathrm{cm}^2\ \mathrm{s}^{-1}$
x	non-dimensional distance along the catalyst layer, $0 \leq x \leq 1$
l	thickness of the CCL, cm
σ	proton conductivity, $\sigma = \sigma_{el}/l$, $\mathrm{S\ cm}^{-2}$
σ_{el}	specific proton conductivity, $\mathrm{S\ cm}^{-1}$
m_{mass}	mass transport coefficient, V
n_{mass}	simulation parameter for the polarization curve fitting, $\mathrm{cm}^2\ \mathrm{A}^{-1}$
b	Tafel slope, V
E	cell voltage, V
E_0	open-circuit voltage (OCV), V
j	current density distribution along the CCL, $\mathrm{A\ cm}^{-2}$

i^*	exchange current density, A cm^{-2}
I	current density, A cm^{-2}
η_1	overpotential at PEM/CCL interface, V
i	imaginary component in impedance
w	frequency, Hz
F	Faradaic constant, 96487 A s mol^{-1}
P	total pressure, Pa
T	temperature, K
R	Gas constant, 8.314 J K^{-1} mol^{-1}

Subscripts

C	constant phase element (CPE)
B	bounded constant phase element (BCPE)
1	PEM/CCL interface
ct	Charge transfer
$ohmic$	ohmic
$mass$	mass transport

k iteration number of the node, $1 \leq k \leq n-1$

n total repeating number of the node

Chapter 1. Introduction

1.1 Background

Due to increasing greenhouse gases, global warming is one of the biggest environmental problems of the 21st century. In addition, 17% of the carbon dioxide emissions comes from the internal combustion engines of cars [2]. For zero-emissions and higher efficiency, automobiles with polymer electrolyte membrane (PEM) fuel cells have gained attention [3]. A PEM fuel cell converts the chemical energy of the reaction between hydrogen (H_2) and oxygen (O_2) into electrical energy with pure water [3, 4]. For that reason, PEM fuel cell technologies have been heavily invested in by automotive companies. Up to now, the Honda Clarity (2008), Mercedes-Benz F-Cell (2010), Toyota Myrai (2014), and Hyundai Nexo (2018) have been introduced to the market. Other corporations have also invested heavily to develop hydrogen techniques.

Identifying the performance and resistance of a fuel cell is helpful when investigating PEM fuel cell, because they can determine the research direction and the appropriate operating conditions. However, it is not easy to investigate these parameters of PEM fuel cells, because these data are closely related to each other. For examples, water contents and oxygen transport mechanism are related to one another in which counteracting interdependencies are accounted for [5]. Oxygen transport is dominantly attributed to the water concentration in the Nafion and gas

diffusion layer (GDL), and the flow channel. Therefore, researchers need precise and detailed information on the PEM fuel cell performance and resistance to identify the research direction and operating conditions.

In order to get this information, researchers have generally used electrochemical impedance spectroscopy (EIS) and polarization curve which provide resistance and current-voltage information, respectively [5, 6]. However, these experimental methods have several limitations when interpreting the fuel cell conditions. EIS results are not always clear in terms of what specific features of the impedance spectrum relate to which physical, chemical, or electrochemical processes and features [5]. The separation method and equivalent circuit also need additional studies. For instance, protonic resistance in the cathode catalyst layer (CCL) has not been sufficiently studied at the middle and high current density regions [7], even though it is essential data for the fabrication of Membrane Electrode Assembly (MEA). In the case of the lumped circuit, it is difficult to describe the resistance in the CCL regardless of the operating conditions. On the other hand, a polarization curve provides the overall performance but no details. Namely, one of these two measurement techniques is not enough to separate the resistance or overpotential at a more detailed level. In this respect, testing techniques that consider both the EIS and polarization curve are needed because it can provide more precise and detailed information by comparing each experimental result.

1.2 Literature review

1.2.1 Electrochemical impedance spectroscopy of PEM fuel cells

The characteristics of a PEM fuel cell can be tested by *ex situ* and *in situ* methodologies. One of the *in situ* methodologies is EIS. This is also called ac impedance [5]. First, the basic concept of this method comes from the alternating expression of the fuel cell using an electrical circuit shown in Figure 1.1. This technique can distinguish the total resistance at a specific point on the polarization curve using the impedance spectrum. In general, an impedance spectrum is plotted in a Nyquist plot, which is a parametric plot as a function of frequency. The real part of the impedance spectrum is plotted on the X-axis, and the imaginary part is on the Y-axis. For visibility, the imaginary value is plotted with a negative sign. The frequency decreases from the left to the right [6]. AC impedance requires some assumptions, system linearity and stability for the facile analysis. Therefore, this technique should be performed on the cell using a small amplitude voltage or current perturbations within 20mV [8].

If the anode resistance is far smaller, the semi-circle related to the anode part cannot be found in the experimental results of the EIS, and the anode part of the equivalent circuit can be neglected. The kinetics of hydrogen oxidation is faster than of the oxygen reduction reaction; thus, the anode resistance can be negligible [9-12]. In addition, the resistance of fuel cell at the cathode can be divided into high

frequency resistance (including the ionic resistance, contact resistance and electronic bulk resistance such as flow field, diffusion media and cable), charge transfer resistance represented by a parallel RC circuit with a double layer capacitance, and mass transport resistance by the diffusion. In this case, various lumped circuits are widely used to fit the experimental results [4, 13-15]. However, a lumped circuit has a limitation in describing the protonic resistance in the CCL, except that potential drop along the pores caused by the electrolyte resistance is small [16].

1.2.2 Protonic resistance in the cathode catalyst layer

Generally, a lumped circuit is useful for approximately evaluating the resistance; thus, this kind of equivalent circuit has been widely used. However, a lumped circuit is not appropriate to describe the region of the protonic resistance in the CCL which represents a 45-degree straight line at the high frequency region around the first semi-circle [7, 17-19]. More specifically, this line pushes away the first arc from the origin and that distance from the x-intercept is proportional to the magnitude of the protonic resistance in the CCL. The distance is called the effective protonic resistance in the CCL [9, 20-24]. To describe this 45-degree straight line, differential equations or the finite transmission-line model (TLM) is normally used to represent a porous electrode more specifically and precisely [7, 25, 26]. The model consists of an electronic resistor rail to explain the path of the electrons and an ionic resistor rail to explain the path of the protons in the CCL. Between these

two rails, capacitors and resistors are located to explain the reaction at the triple phase boundary (TPB). Occasionally, the reaction part of the TLM also includes the Warburg impedance to describe the diffusion process [1].

Meanwhile, Makharia et al. [7] reported the calculation of the effective protonic resistance using a differential equation and analyzed the results of H_2/N_2 experiments under low current densities. The sum of all the distributed proton transport resistances estimated from the TLM was approximately equal to three times the effective protonic resistance. However, in this process, the homogeneity of the distributed elements in the TLM was assumed, and the experiments were carried out at low current density. In this respect, Malevich et al. [27] studied the effect of distributed proton transport resistances in the CCL. When the distributed protonic resistances were non-uniform in the H_2/N_2 experiments, the effective protonic resistance in the CCL was not one third of the protonic resistance in the CCL. In addition, the line starting from x-intercept at the high frequency region was also not a clear 45-degree straight line. To be brief, the 45-degree straight line appeared when the distribution of the protonic resistance in the CCL was homogenous in the H_2/N_2 experiments. In this condition, the effective protonic resistance was approximately one third of the protonic resistance in the CCL. However, these were based on the H_2/N_2 experiment; thus, it cannot consider the effect of water generation in the H_2/air condition. The operating condition was also limited at the low current density region.

Furthermore, Gerteisen [28] additionally studied the impact of the inhomogeneity of the charge transfer resistance in the H_2/air condition which affected the charge transfer arc. Because the non-uniformity of the charge transfer resistance affected the total resistance, Gaumont et al. [21] suggested a general solution which included a non-uniform distributed charge transfer resistance in the CCL. The general solution was derived using an equivalent circuit with the current distribution through the thickness of the electrode. Therefore, as the distance from the membrane was altered, the distributed charge transfer resistances were also changed. Consequently, when the protonic resistance in the CCL was less than or equal to the charge transfer resistance, the Nyquist plot with a small current approximation was almost similar to the general solution. However, when the protonic resistance was much larger than the charge transfer resistance, the approximated solution was represented as a much bigger semi-circle than that of the general solution. Although that work considered the variation in the distributed charge transfer resistance, the equivalent circuit did not take into account the effect of the mass transport resistance or the diffusion effect.

Cruz-Manzo and Chen [25] suggested using the TLM together with the Bounded Warburg to reflect the diffusion effect in the catalyst layer under the whole current density region [29]. That paper evaluated the differential equations and suggested the electrical equivalent circuit, but an estimation with a recursion formula was not attempted. To solve the differential equations, it was assumed that the protonic resistance in the CCL should be much smaller than the charge transfer resistance.

Therefore, even though these equations were derived without the current density restriction [29], the assumption should be satisfied to use the formula under the whole current density region. However, the formula was also derived under the assumption. For a clear estimation, the formula and resistance should be validated first using other methodologies or exact solutions. Moreover, that paper did not identify the relationship between the effective protonic resistance and the protonic resistance.

1.2.3 Effect of the current density and relative humidity on the resistance

The current density and relative humidity (RH) are the most important variables in the operation of PEM fuel cells. These conditions critically affect the performance. Several works have been devoted to the study of the current density and relative humidity. Mann et al. [30] suggested an increase in the membrane resistance with the current density using prediction of a generalized steady-state electrochemical model. Cooper and Smith [31] compared the ohmic resistances determined by the current interrupt, polarization curve, and EIS experiments. All of them increased, as the current density was increased, even though each value of the resistance was not exactly the same. Andreaus [32] also measured the ohmic resistance with the current density using EIS and the current pulse method. Furthermore, the change in the ohmic resistance was described with a polarization curve to refer to the condition of the PEM fuel cell. At a high current density, as the

anode overpotential increases, the membrane resistance is increased due to the drying out of the electrolyte adjacent to the anode. Meanwhile, Xu et al. [33] investigated the effect of temperature and RH on the kinetics of the oxygen reduction reaction. A reduced RH increased the Tafel slope due to changes in the ORR pathways, proton activity, and catalyst surface condition. Brunetto et al. [4] measured the variation of the resistance by the RH change. As the RH was increased, the ohmic resistance, charge transfer resistance, and mass transport resistance decreased under the low current density condition.

In contrast, further research is required on the change in protonic resistance with the operating condition. Although the proton conductivity [34-37] and water content [21, 38, 39] in the CCL have been investigated, there are few studies on the effect of the relative humidity and the current density on the effective protonic resistance in the CCL under the H_2/air condition.

1.2.4 Correlation of EIS with polarization curve

While EIS provides detailed information on each resistance, polarization curve has also been commonly used to investigate the general quantification of performance [5]. Because each of these two experiments provides different information, several researchers have used both of them [4, 31, 40].

Wagner [41] mentioned the correlation between AC impedance and the polarization curve. The polarization resistance of the fuel cell was tangent to the

polarization curve at a specific potential. Moreover, the total resistance also can be measured using AC impedance at a frequency near 0Hz, because this measurement condition was very similar to the DC condition. To obtain the total resistance, two methods were suggested in that paper. First, one was an estimation of the EIS impedance at a very low frequency through extrapolation, and the second method was summation of the individual resistances.

Tang et al. [42] compared the cell voltage drop due to each resistance using EIS and polarization curve. To compare the two experimental results, each resistance was evaluated by EIS, and then, the percentage of the voltage drop was estimated and compared to the polarization curve. Consequently, that paper suggested a methodology to compare the EIS with the polarization curve using the resistance; however, the protonic resistance in the CCL wasn't considered.

1.3 Objective

Several works have been done using EIS and polarization curve. However, the estimation of each resistance (including the charge transfer resistance, high frequency resistance, mass transport resistance, and effective protonic resistance in the CCL) based on EIS and polarization curve could not be sufficiently carried out due to a deficiency in the methodologies to separate the resistance. In this study, the four types of resistances were considered to derive the general solution of the impedance model. From this general solution, a new method was proposed to separate the total resistance. When the distributed elements in the TLM were homogeneous and the distributed protonic resistance in the CCL was less than the summation of the distributed charge transfer resistance and mass transport resistance, each resistance can be evaluated only by EIS. In another case, the correlation between the EIS and the polarization curve was used. Consequently, the total resistance in a PEM fuel cell was quantitatively separated. It was conducted under different current densities and relative humidity conditions, and then the variations of the resistance were analyzed to ensure the reliability of the results. After that, the overpotentials caused by each resistance were estimated to understand the effect of the resistance in terms of the voltage.

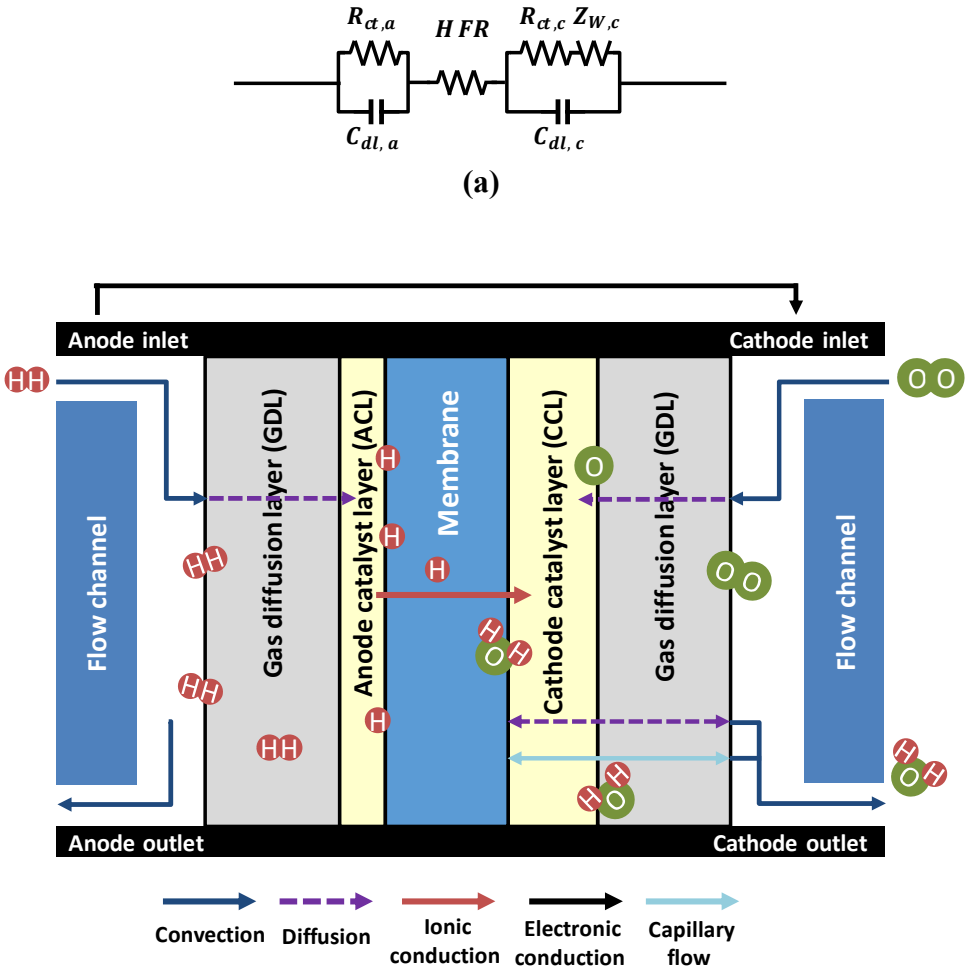

Figure 1.1 (a) Electrical equivalent circuit for a simple PEM fuel cell impedance model. R_{ct} is a charge transfer resistance, Z_{mass} is a Warburg, HFR is a high frequency resistance and C_{dl} is a double layer capacitance. (b) A schematic of the cross-section view of a PEM fuel cell (not to scale)

Chapter 2. Experimental setup and assumptions

2.1 Experimental setup

The measurements for the EIS and the polarization curve were done in the experimental conditions listed in Table 2.1. Before measuring the EIS data, the voltage and current density were measured to plot the polarization curve; because the EIS and polarization curve were measured in the same operating condition, as far as possible. For these experiments, a FC Impedance Meter (KIKUSUI, KFM 2150 and PLZ-4W) was used. To satisfy the EIS assumptions such as linearity and stability, a potential amplitude should be maintained at less than 10 mV. For an AC sinusoidal signal, the analyzed frequency range was 20 kHz to 900 mHz. However, to ensure the existence of another semi-circle appearing around the low frequency, the end frequency was 10 mHz in the high current density region. The electronic bulk resistance and contact resistance in the high frequency resistance (HFR) were measured using an *ex situ* dc experiment with a PEM fuel cell except for the MEA. This measurement can consider the whole electronic bulk resistance and contact resistance except for the MEA. To measure the electrical resistance, a milliohm (GWINSTEK, GOM-802) was used. The temperature and pressure were kept at 65 ℃ and ambient pressure, respectively.

Table 2.2 lists the materials of the fuel cell used in this work. The 1 cm^2 active area near the outlet of the 25 cm^2 flow channel was assembled by using a gasket

and GDL shown in Figure 2.1 which provides in-plane uniformity of the resistance, current distribution, and reactant gas. Thus, a single cell was used to control the operating condition as well. Figure 2.2 shows an overview of the components of the PEM fuel cell.

2.2 Experimental conditions and assumptions

Unlike other fuel cell experiments, EIS and polarization curve require high stoichiometry ratios (SR) and a small active area for several assumptions as follows. These assumptions were related to the impedance model.

- The SR has to be kept high to minimize reactant depletion along the channels. This setup also makes a high diffusion condition though the CCL.
- The active area of the fuel cell needs to be small to have a uniform pressure and velocity.

As mentioned later, this study used the current distribution equation, Eq. (7), which assumes a fast oxygen diffusion. For this reason, a high SR condition was used. The RH of the inlet gas was changed from 50% to 100% to investigate the effect on each resistance. The current was varied from 0.1 to 2.4 A/cm^2 at 0.1A/cm^2 increments to compare the EIS and polarization curve results. Almost all experimental cases were conducted under the H_2/air condition; however, the H_2/Heliox (21 % O_2 with the balance made up of He) was also carried out to identify the diffusion effect of oxygen.

Table 2.1 Operating conditions for measuring the EIS and polarization curve

Parameter	Condition
Test mode	Galvanostatic technique
Frequency	20 kHz to 900mHz
Swing width of AC current	within a voltage amplitude of less than 10 mV
Current density	0.1 ~ 2.4 A/cm^2
Mass flow	Anode: 0.400 ln/min (SR* > 20) Cathode: 2.00 ln/min (SR* > 40)
Reactant gas	H_2/air H_2/Heliox(21 % O_2, 87% He)
Inlet gas RH**	50, 80, 100 % (anode/ cathode)
Cell temperature	65 ℃
Outlet pressure	Ambient pressure

* Stoichiometric Ratio

** Relative Humidity

Table 2.2 Components used for the experiments.

Component	Condition
Flow Channel	Parallel channels (anode/ cathode) 1/0.815 mm width (channel/rib) 0.4/0.6 mm depth (anode/cathode)
GDL-MPL	JNT30-A6H (Thickness 325 ± 5 μm)
MEA†	GORE™ PRIMEA® 5730‡

†Membrane Electrode Assembly

‡Catalyst Coated Membrane

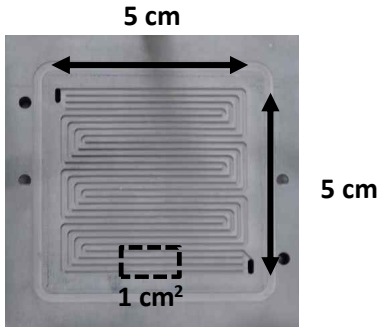

(a)

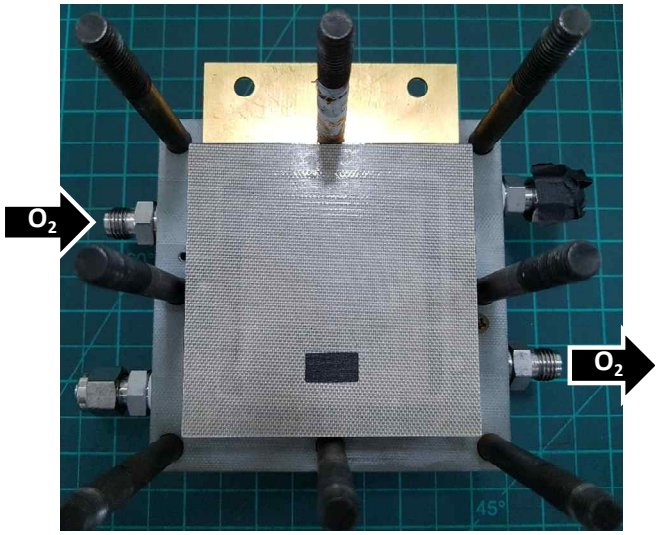

(b)

Figure 2.1 Setup of the active area. (a) Flow channel (b) Assembly of end plate, flow channel, gasket and GDL

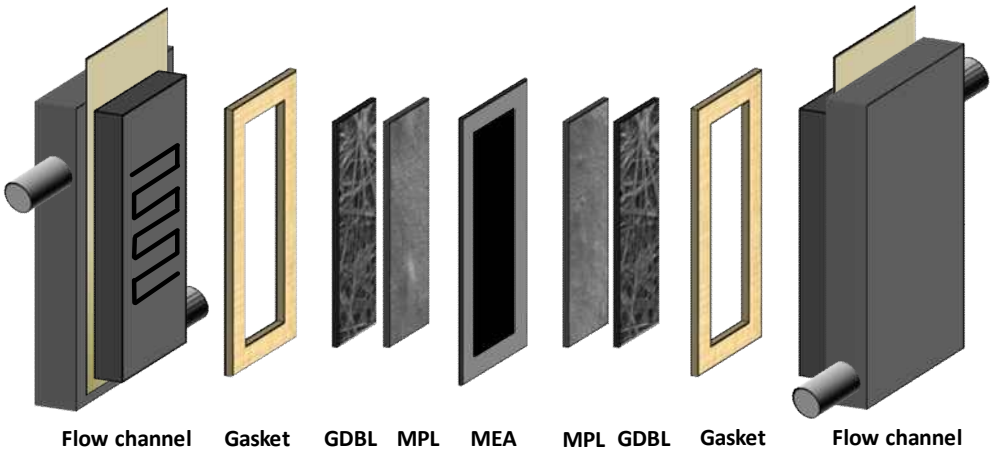

Figure 2.2 A schematic of the components in a PEM fuel cell (not to scale)

Chapter 3. Impedance model

3.1 Electrical equivalent circuit

Reasonable selection of an electrical equivalent circuit is an essential step before analyzing the experimental data. The kinetics of the hydrogen oxidation reaction is faster than that of the oxygen reduction reaction; thus, the anode resistance can be negligible [9-12]. In addition, the ohmic resistance caused by the electron flow in the CCL can be negligible, because the electronic resistance in the CCL is smaller than that of the ionic resistance. Conclusively, the anode resistance and electronic resistance in the CCL were not critically shown in our experimental results. Thus, the anode part and the electronic resistances in the CCL were neglected as in previous studies [7, 9-12, 21]. Unlike other equivalent circuits, the bounded constant phase element (BCPE) in the TLM was needed to represent the mass transport effect in the CCL. Thus, the equivalent circuit suggested by Cruz-Mano et al. [1] was used in this work. To improve the fitting results, the Bounded Warburg was replaced by the BCPE, and the element of the inductor was eliminated shown in Figure 3.1.

HFR includes the electronic bulk resistance, contact resistance and the resistance by the proton conduction in the membrane. The TLM, shown in Figure 3.1, represents the catalyst layer, which includes the distributed protonic resistance in the CCL (r_p), distributed charge transfer resistance (r_{ct}), distributed BCPE (z_W),

and constant phase element (CPE) for the double-layer capacitance. n is the total repeating number and k is the iteration number of the node in the interval ($1 \leq k \leq n-1$). Referring a previous paper, n is one thousand [21].

3.2 General solution

To represent the Nyquist plot with the TLM, general solution was used with recursion formula [21]. The CCL part of the Nyquist plot can be evaluated iteratively using the recursion formula from the CCL/GDL interface to the PEM/CCL interface as follows:

$$\begin{aligned} Z_n &= \frac{z_{ct,n}}{\delta x} + r_{p,n}\delta x \\ Z_k &= \left(\frac{1}{Z_{k+1}} + \frac{1}{\frac{z_{ct,k}}{\delta x}} \right)^{-1} + r_{p,k}\delta x \ , \quad r_{p,1} = 0 \end{aligned} \tag{1}$$

with

$$\delta x = \frac{l}{n} \tag{2}$$

$$CPE_k = q_{C,k}(i\omega)^{P_{C,k}} \tag{3}$$

$$z_{ct,k} = \left[\left\{ r_{ct,k}\delta x^2 + z_{W,k}\delta x^2 \right\}^{-1} + CPE_k \right]^{-1} \tag{4}$$

$$z_{W,k} = \frac{\tanh(r_{mass,k}\delta x^2 q_{B,k}(i\omega)^{P_{B,k}})}{q_{B,k}(i\omega)^{P_{B,k}}\delta x^2} \tag{5}$$

where l, x, r_{mass}, q_C, P_C, i, ω, q_B and P_B are, respectively, the thickness of the CCL, the non-dimensional distance along the CCL ($0 \le x \le 1$), the distributed mass transport resistance, the distributed parameter related to the CPE, the CPE exponent, the imaginary component in the impedance, the frequency, the distributed parameter related to the BCPE and the BCPE exponent.

To apply the inhomogeneity of r_{ct}, r_{ct} is calculated by [21, 43]

$$r_{\alpha,k} = \frac{b}{j(x)}\frac{1}{\delta x^2} \tag{6}$$

with

$$j(x) = \frac{\sqrt{2i^*\sigma b}}{l} \cdot \exp\left(\frac{\eta_1}{2b}\right) \cdot \tan\left(\sqrt{\frac{i^*}{2\sigma b}}(1-x)\exp\left(\frac{\eta_1}{2b}\right)\right) \tag{7}$$

where b is the Tafel slope; σ is the proton conductivity; i^* is the exchange current density and η_1 is the overpotential at the PEM/CCL interface.

This equation can be used under the assumption that oxygen diffusion is fast. Although this assumption is satisfied by the high SR condition, a single parameter is used to be sure.

$$g = \frac{4FPD^{eff}}{RTl}\frac{1}{\sigma b} \tag{8}$$

It was estimated as 14 ~ 250 based on the experimental results. Thus, Eq. (7) can be used in this study because $g \gg 1$.

3.3 Resistance separation using EIS

The general solution with the recursion formula was derived in the last section. However the distributed resistance from the general solution is not convenient to separate the total resistance (R_{total}). To divide R_{total} into the effective protonic resistance in the CCL (R_p^{eff}), the charge transfer resistance (R_{ct}), and the mass transport resistance (R_{mass}) using the distributed elements, three assumptions were applied [16].

- The distributed elements are homogeneous.
- $r_p/(r_{ct} + z_W) \ll 1$.
- As previously mentioned, the anode resistance and electronic resistance in the CCL are neglected.

R_{total} is the most important information in this study. Thus, a point of intersection in the real axis at a low frequency is extracted from the Eq. (1) [41].

$$R_{total} = \lim_{w \to 0}(HFR + Z_1) = HFR + \frac{r_{ct}\,\delta x + r_{mass}\delta x}{A_{n-1} + 1} + r_p \delta x \tag{9}$$

with

$$A_{n-k} = \frac{(A_{n-k-1}+1)(r_{ct}+r_{m\,ass})}{(r_{ct}+r_{m\,ass})+(A_{n-k-1}+1)r_p}\,, \quad A_0 = 0 \tag{10}$$

Then, a general term can be derived as follows. From the Eq. (10),

$$A_{n-k} = A_{n-k-1} + 1 - \frac{r_p}{r_{ct}+r_{m\,ass}} \cdot \frac{(A_{n-k-1}+1)^2}{1+(A_{n-k-1}+1)\cdot\dfrac{r_p}{r_{ct}+r_{m\,ass}}} \tag{11}$$

By the second assumption,

$$A_{n-k} \approx A_{n-k-1} + 1 - \frac{r_p}{r_{ct}+r_{m\,ass}} \frac{(A_{n-k-1}+1)^2}{1} \tag{12}$$

When k is large, Eq. (11) can be approximated more simply as shown below because both $r_p/(r_{ct}+z_W)$ and $(A_{n-k-1}+1)^2$ are small

$$A_{n-k} \approx A_{n-k-1} + 1 \tag{13}$$

$$\approx n-k \tag{14}$$

Therefore, the right hand side of the Eq. (12) can be simplified as Eq. (15) by Eq. (14). At this point, the error by Eq. (14) is only acceptable when k is large. Therefore, the error in the third term on the right hand side can be approximated using Eq. (14) due to $r_p/(r_{ct}+z_W)$. However, Eq. (14) does not apply to the first term on the right hand side, because the error in this term is not negligible without multiplication of $r_p/(r_{ct}+z_W)$.

$$A_{n-k} \approx A_{n-k-1} + 1 - \frac{r_p}{r_{ct} + r_{m\,ass}} \cdot (n-k)^2 \tag{15}$$

Finally, the general term of the recursion formula can be derived from Eq. (15).

$$A_{n-k} \approx n - k - \frac{r_p}{r_{ct} + r_{m\,ass}} \frac{(n-k)(n-k+1)(2n-2k+1)}{6} \tag{16}$$

The general term can be derived by substituting Eq. (16) into Eq. (9).

$$R_{total} = HFR + \frac{r_{ct}\,\delta x + r_{m\,ass}\delta x}{n - 1 - \frac{r_p}{r_{ct} + r_{m\,ass}} \frac{(n-1)(n)(2n-1)}{6} + 1} + r_p \delta x \tag{17}$$

When the first assumption is valid, Eq. (17) can be rearranged as follows [9, 41].

$$\begin{aligned} R_{total} &= R_{ct} + R_{ohmic} + R_{m\,ass} \\ &= R_{ct} + HFR + R_P^{eff} + R_{m\,ass} \end{aligned} \tag{18}$$

with

$$R_P^{eff} = \frac{\frac{r_p \delta x\,(n-1)(2n-1)}{6n}}{1 - \frac{r_p}{r_{ct} + r_{m\,ass}} \frac{(n-1)(2n-1)}{6}} + r_p \delta x \tag{19}$$

$$R_{ct} = \frac{r_{ct}\,\delta x}{n} \tag{20}$$

$$R_{m\,ass} = \frac{r_{m\,ass}\delta x}{n} \tag{21}$$

where R_{ohmic} is the ohmic resistance of the summation of HFR and R_P^{eff}.

3.4 Validation of the recursion formula

In this section, the general solution (Eqs. **(1)** - (7)) and the general term (substituting Eq. (16) into Eq. (9)) were validated using the solution suggested by Cruz-Manzo and Chen [1] and by experimental results.

Cruz-Manzo and Chen [1] suggested not only an equivalent circuit but also a solution of differential equations for the impedance model as depicted in Figure 3.1. This solution, the validation model, was used to validate the general solution. After disregarding the inductance term and replacing the Bounded Warburg with the BCPE, the final total impedance equation can be written as

$$Z_{total} = HFR + \frac{[R_{ct} + Z_W]\gamma_1 \coth(\gamma_1(1-x))}{1 + Q_C(i\omega)^{P_C}[R_{ct} + Z_W]} \tag{22}$$

with $\gamma_1 = \sqrt{R_p\left[\frac{1}{R_{ct}+Z_W} + Q_C(i\omega)^{P_C}\right]}$

$$Z_W = \frac{\tanh(R_{mass}Q_B(i\omega)^{P_B})}{Q_B(i\omega)^{P_B}} \tag{23}$$

where R_p is the protonic resistance in the CCL; Z_W is the BCPE; Q_C is the parameter related to the CPE and Q_B is the parameter related to the BCPE. To derive Eq. (22), it was assumed that the element in the CCL was homogeneous. Furthermore, to satisfy the homogeneity of r_{ct}, Eq. (24) should be valid [1].

$$\frac{R_p}{R_{ct}} \ll 1 \quad (24)$$

Figure 3.2 shows the fitting results of the general solution and the validation model. Both models fitted well with the experimental results regardless of the current densities. However, the general solution no longer fitted well with the validation model at RH 50%. The reason for these results can be found from the assumption on the homogeneity of r_{ct}. $r_p/(r_{ct} + z_W)$ was much smaller than 1 ($3.5 \times 10^{-7} > r_p/(r_{ct} + z_W) > 7.6 \times 10^{-8}$) regardless of the RH conditions; thus, it seems that the reason for the mismatch at RH 50% was caused by the inhomogeneity of r_{ct} in TLM. As a result, the homogeneous assumption of r_{ct} can be valid under RH 80% and 100%.

On the other hand, because the straight line in our experimental data was kept at 45-degrees, it seems that the impacts of the inhomogeneity of the double layer capacity and protonic conductivity might not be significant as in previous research [28].

Furthermore, the validation of the general term was done with R_{total} which was evaluated with the experimental data. By comparing the R_{total} from the general term and from the general solution, the error of general term was less than 1% under RH 100% regardless of the current density. However, the error increased as the RH was decreased. The maximum error at the RH 80% was around 1.5%. Therefore, the error caused by the assumption $r_p/(r_{ct} + z_W) \ll 1$ was not significant under RH 80%, 100%. Consequently, resistance separation can be

carried out by Eqs. (18) - (21) when the TLM is homogeneous, and the RH is over 80%.

In addition, $R_P^{eff} \approx R_p/3$ can be derived. From the Eq. (19),

$$R_P^{eff} = \frac{\frac{r_p \delta x\,(n-1)(2n-1)}{6n}}{1-\frac{r_p}{r_{ct}+r_{m\,ass}}\frac{(n-1)(2n-1)}{6}} + r_p \delta x \tag{19}$$

Because $n \gg 1$ (in this study, n is 1000), $n \approx n-1 \approx \frac{2n-1}{2}$.

$$R_P^{eff} \approx \frac{\frac{n r_p \delta x}{3}}{1-\frac{r_p}{r_{ct}+r_{m\,ass}}\frac{n^2}{3}} + r_p \delta x \tag{25}$$

If $r_p \delta x^{\,2}/(r_{ct}+z_W) \approx 0$ and $r_p \delta x \ll \frac{n r_p \delta x}{3}$,

$$\begin{aligned} R_P^{eff} &\approx \frac{r_p \delta x \left(1-\frac{r_p}{r_{ct}+r_{m\,ass}}\frac{n^2}{3}\right)+\frac{n r_p \delta x}{3}}{1-\frac{r_p}{r_{ct}+r_{m\,ass}}\frac{n^2}{3}} \\ &\approx \frac{n r_p \delta x}{3} \\ &\approx \frac{R_p}{3} \end{aligned} \tag{26}$$

3.5 Resistance separation using the correlation between the EIS and polarization curve

In some cases, the approximation of $r_p/(r_{ct} + z_W)$ or the assumption on the homogeneity of r_{ct} may not be valid. The results of middle or high current densities under the H_2/Heliox condition showed that the assumption $r_p/(r_{ct} + z_W) \ll 1$ was not correct because R_{mass} was low due to the high diffusion coefficient. This section suggests another methodology for this condition, because the resistance separation by Eqs. (18) - (21) is no longer available. For this reason, the correlation between EIS and polarization is applied to separate the resistance. Naturally, resistance separation can be done with only a polarization curve [42]; however, an additional analysis of the EIS results is helpful to consolidate the validity of the resistance separation.

The polarization curves, shown in Figure 3.3, are expressed using a semi-empirical equation [44]:

$$E = E_0 - b\ln(I \cdot 10^3) - IR_{ohm\,ic} - m_{mass}\exp(n_{mass}I) \quad (27)$$

where E is the cell voltage; E_0 is the open-circuit voltage (OCV); I is the current density; m_{mass} is the mass transport coefficient and n_{mass} is the simulation parameter for the polarization curve fitting. For resistance separation based on Eq. (27) [9],

$$
\begin{aligned}
R_{total} &= R_{ct} + R_{ohmic} + R_{mass} \\
&= \frac{dE}{dI} \\
&= \frac{b}{I} + R_{ohmic} + m_{mass} n_{mass} \exp(n_{mass} I) \\
&= \frac{b}{I} + HFR + R_P^{eff} + m_{mass} n_{mass} \exp(n_{mass} I)
\end{aligned}
\tag{28}
$$

HFR is evaluated by EIS regardless of the current density region. Meanwhile, R_{ct} and R_{mass} are estimated by the EIS and polarization curve. In general, at a low current density region, the approximation of $r_p/(r_{ct} + z_W)$ and the assumption on the homogeneity of r_{ct} can be used [7, 21]. Thus, the unknown parameter in Eq. (27), such as E_0, b, m_{mass} and n_{mass}, are determined by the experimental data of the EIS under low current densities. By Eq. (28), the R_{ct} and R_{mass} can be estimated, when $r_p/(r_{ct} + z_W)$ is large, or r_{ct} is not homogeneous. Finally, R_P^{eff} can be evaluated by Eq. (28) because the total resistance is found by the EIS and polarization curve. Consequently, although $r_p/(r_{ct} + z_W)$ is not small and r_{ct} is not homogeneous, the resistance can be separated using Eq. (28) and the fitting results on the other current density region.

Table 3.1 Summary of solutions

	R_p* and R_{mass}**	Inhomogeneity of elements	Resistance separation
Solution suggested by SCM	Considered	Not considered	Facile
General solution	Considered	Considered	Arduousness
Approximated solution with homogeneous elements	Considered	Not considered	Facile
Approximated solution with inhomogeneous elements	Considered	Considered	Facile

* Protonic resistance in cathode catalyst layer
** Mass transport resistance

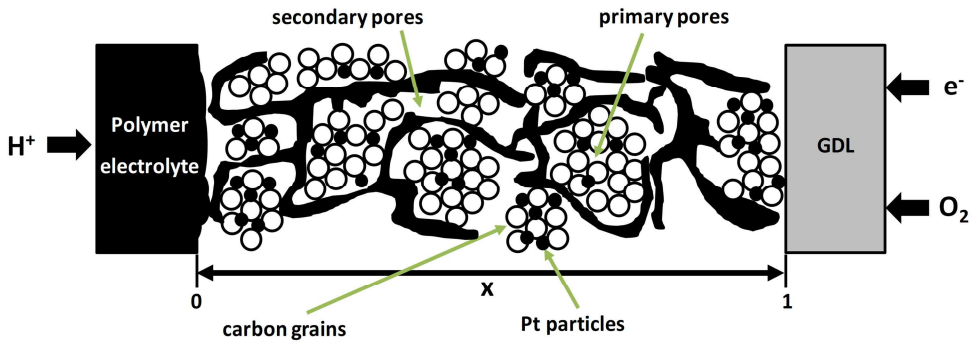

(a)

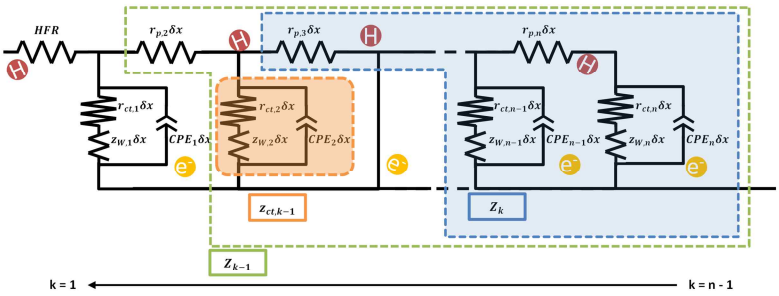

(b)

Figure 3.1 (a) A schematic of the CCL. $\boldsymbol{x}$ represents the non-dimensional thickness of the CCL from CCL/GDL interface ($\boldsymbol{x = 0}$) to the PEM/CCL interface ($\boldsymbol{x = 1}$). (b) Electrical equivalent circuit of a PEM fuel cell represented by a TLM [1].

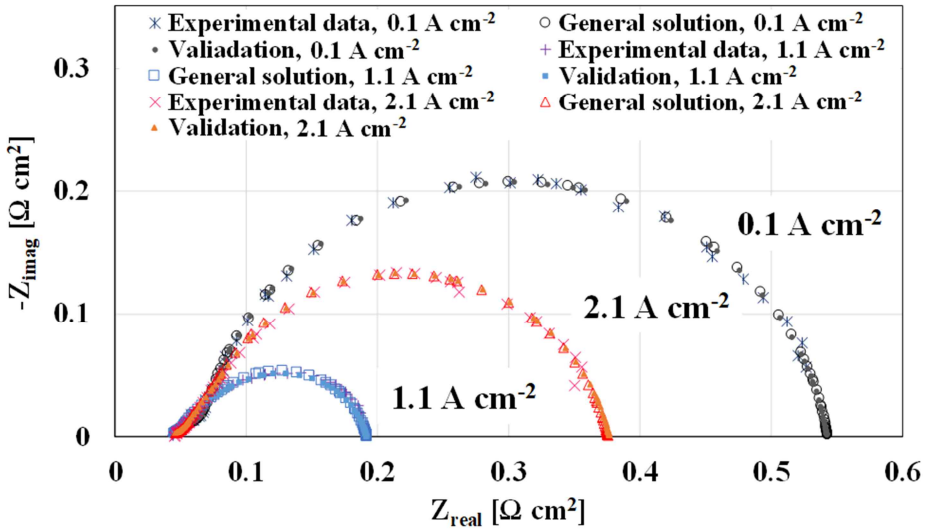

(a)

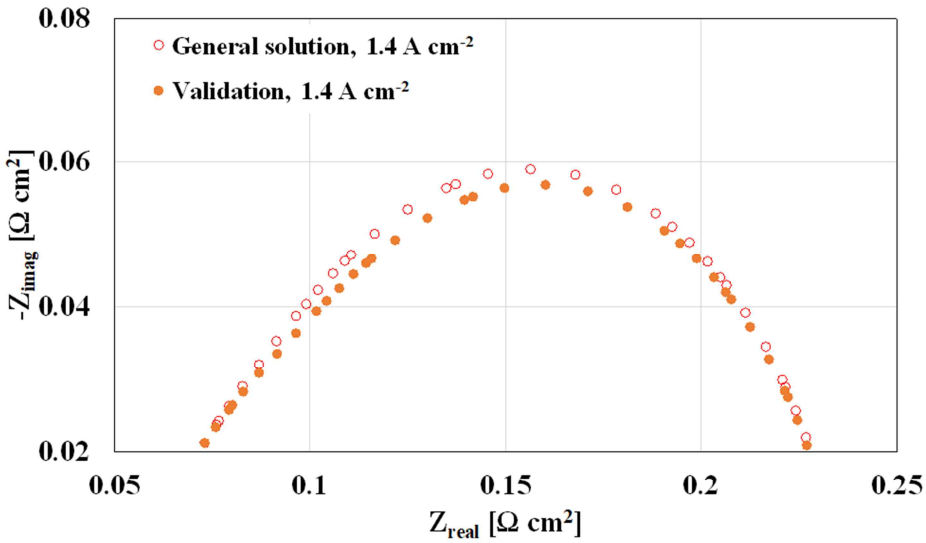

(b)

Figure 3.2 (a) Nyquist plots are plotted at RH 100%, (b) RH 50% under H_2/air condition. Open symbols represent general solution and closed symbols represent validation model. Cross symbols represent experimental data.

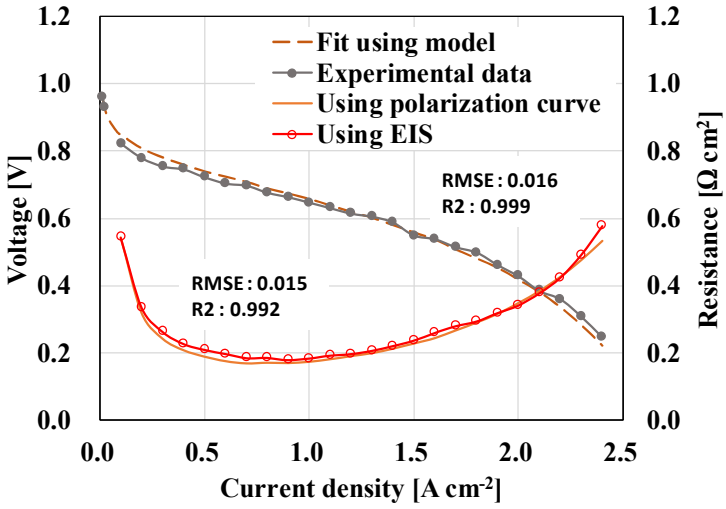

(a)

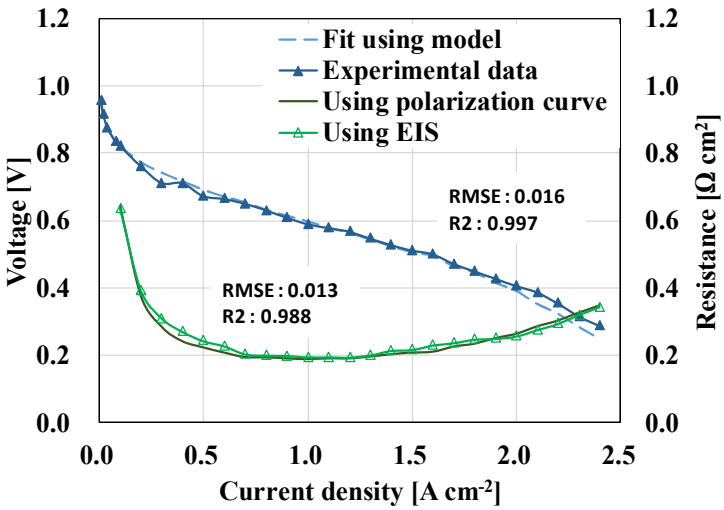

(b)

Figure 3.3 Polarization curves and total resistances at (a) RH 100%, (b) RH 80% under H_2/air experiments. The experimental data of polarization curves were fitted using semi-empirical model. The total resistances using EIS were matched with the total resistances using polarization curves.

Chapter 4. Experimental results and discussion

4.1 Comparison of the EIS and the polarization curve

As shown in Figure 3.3, the polarization curves by our experimental results were well matched with fitting Eq.(27). Differentiating the fitting equation with respect to I gave the information on the resistance as mentioned in chapter 3. Those results were also well matched with the experimental data of the EIS shown in Figure 4.1 ($R^2 > 0.995$ and RMSE < 0.01). As reported by previous studies [33, 45], the R_{ct} increased as the RH decreased. The R_{mass} under RH 100% was larger than that under RH 80% in high current density region; however, these results were not maintained in the low current density region [4, 35, 46]. Furthermore, from the results of the R_{ohmic} at low current densities shown in Figure 4.2, the generated water in the CCL also affected R_{ct} and R_{mass} due to the change in the ORR pathways, proton activity, and the catalyst surface condition [33].

4.2 Comparison of the effective protonic resistance in the CCL and the membrane resistance with the RH and current density

Before the discussion, it is assumed that the electronic bulk resistance and contact resistance in HFR were constant with the RH and current density. It means that the change of HFR was caused by the variation of the membrane resistance. As shown in Figure 4.2 (a), (b), the $R_{ohm\,\dot{c}}$ was divided into HFR and R_P^{eff} by the EIS and polarization curve under the H_2/air experiments. It is already well known that the protonic resistance in Nafion is mostly determined by the water content [47, 48]. In addition, the water content was closely related to the RH and current density. In terms of the RH and current density, the $R_{ohm\,\dot{c}}$ definitely changed due to the R_P^{eff}, but HFR was just a little affected. In other words, compared with HFR, the change of R_P^{eff} was more sensitive to the operating current density and RH condition because of the water content. Furthermore, the change of R_P^{eff} was also highly related to the mean distance of the ionic transport. As the current density was increased, the reaction rate and proton flow also increased. It means, in the low current density region, the effect of the water content increasing by the reaction was more critical than the proton flow increasing. This effect was equilibrated around the middle current density region; thus, the R_P^{eff} became constant. After that, R_P^{eff} increased again due to the high proton flow in the high current density region.

Additionally, the lowest level of R_P^{eff} was almost the same at the identical current densities (1.3 ~ 1.8A cm^{-2}) regardless of the RH condition. It seems that the CCL was fully hydrated at these operating conditions, even though the RH was 80%.

The summation of the electronic bulk resistance and contact resistance in HFR was $0.026\Omega cm^2$. It is a reasonable value when compared to that in a previous paper [7]. By this measurement, protonic resistance in the membrane can be evaluated. Therefore, the protonic resistance in the membrane was bigger than in the CCL under the middle and high current density regions shown in Figure 4.2 (a), (b). One of the reasons can be found in the thickness. The thickness of the MEA was measured using scanning electron microscope (SEM) image. As shown in Figure 4.2 (d), the membrane was $15.00 \pm 1.5\mu m$, and the CCL was $10.91 \pm 1.5\mu m$. Beased on ohm's law, the resistance in the membrane should be bigger as in the experimental results. The second reason can be found in the diffusion effect and the distance of the proton flow. The protons migrated though the electrolyte, but the distance changed with the diffusion of the reactant gas and the proton conductivity. In the membrane, the protons should migrate from the anode to cathode; thus, the movement distance was greater than or equal to the thickness of the membrane. However, in the CCL, the movement distance of the proton was less than or equal to the thickness of the CCL, because O_2 also migrated to the TPB. For this reason, the effective diffusion coefficient (D^{eff}) can affect the R_P^{eff}. To ensure this effect, a H_2/Heliox experiment was conducted to vary the D^{eff} shown in Figure 4.2 (c).

As a result, R_P^{eff} at a high current density was decreased because the movement distance of the proton flow in the CCL was decreased. In other words, several reactant points were moved to the nearby membrane.

Eq. (26) is well-known equation to evaluate the R_P^{eff}. This equation can be derived from Eq. (19), and the error also can be estimated. To derive the equation, $r_p/(r_{ct} + z_W)$ was assumed to be very small ($r_p/(r_{ct} + z_W) \approx 0$). It was stricter than the assumptions with Eq. (18). Therefore, the error due to the assumptions with Eq. (18) was less than 1.5%, but the error due to Eq. (26) was more than 5.8% under RH 80% and 7.1% under RH 100%. In this context, R_P^{eff} was roughly $R_p/3$, but this assumption did not validate well under the main-operating load shown in Figure 4.3.

4.3 Analysis of the overpotential

The new separation methodology is advantageous that it can easily estimate the overpotential and identify the effect of the resistance in terms of the voltage using Eq. (27). Because the polarization curves were well matched with Eq.(27), the overpotential can be calculated using the equation. This calculation was more reliable because this calculation considered the R_P^{eff}. Figure 4.4 suggests the overpotential in regard to the effect of each resistance under different current densities and RH conditions. Consequently, the overpotential by R_{ct} was crucially high. However, the portion of the value decreased as the other overpotential increased by R_{ohmic} and R_{mass} At the low current density, the overpotential by R_{ohmic} was not big. After this region, the overpotential increased as the current density increased.

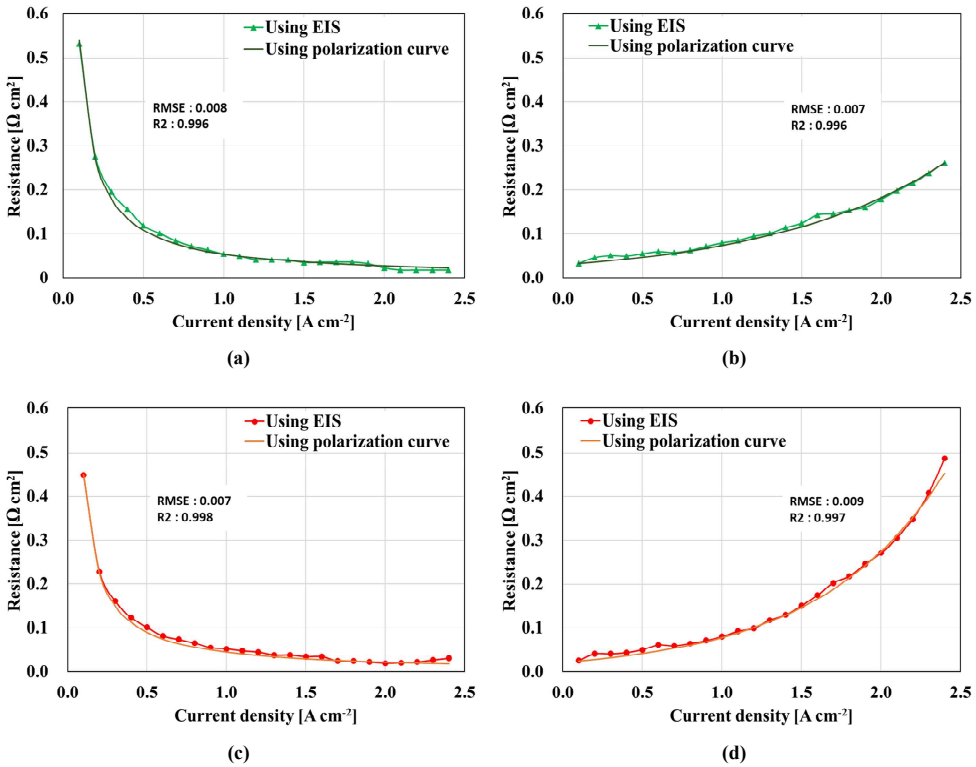

Figure 4.1 Results of the resistance separation under H_2/air. (a) Charge transfer resistance at RH 80%. (b) Mass transport resistance at RH 80%. (c) Charge transfer resistance at RH 100%. (d) Mass transport resistance at RH 100%.

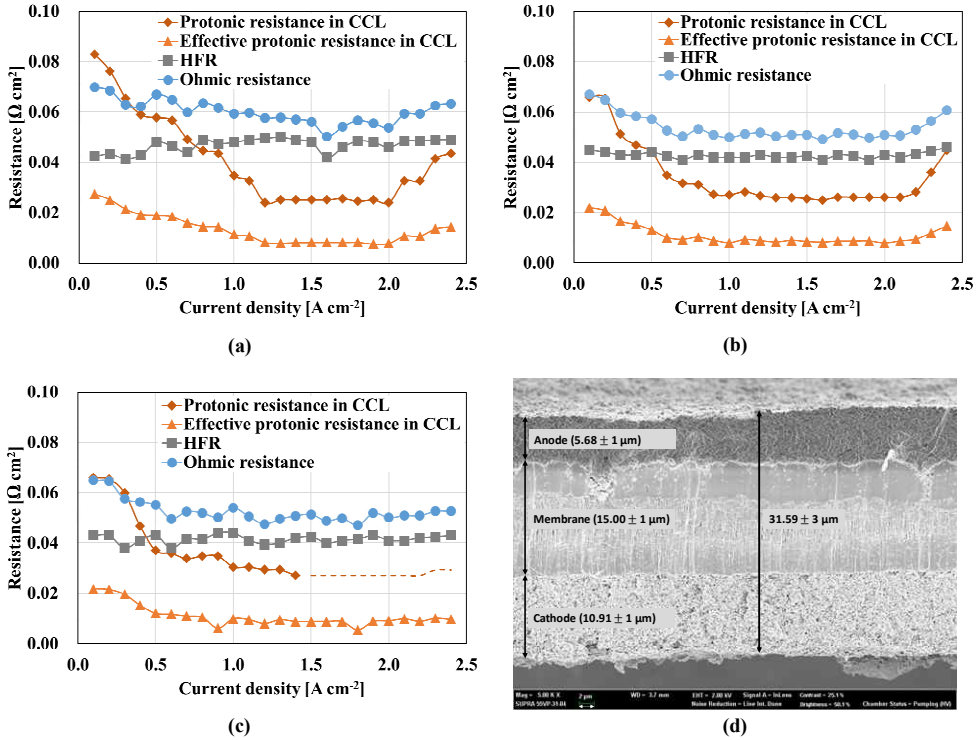

Figure 4.2 Separation of the ohmic resistance at (a) RH 100% under H_2/air, (b) RH 80% under H_2/air, and (c) RH 100% under H_2/Heliox. Rhombus symbol is the protonic resistance in CCL, triangle symbol is the the effective protonic resistance in CCL, square symbol is the high frequency resistance and circle symbol is the ohmic resistance. At the dotted line, fitting of the EIS wasn't well fitted, so protonic resistance in CCL can't be evaluated. In this region, resistance separation was conducted using the correlation between EIS and polarization curve. (d) Cross-sectional SEM image of GORE^{TM} PRIMEA® 5730 CCM.

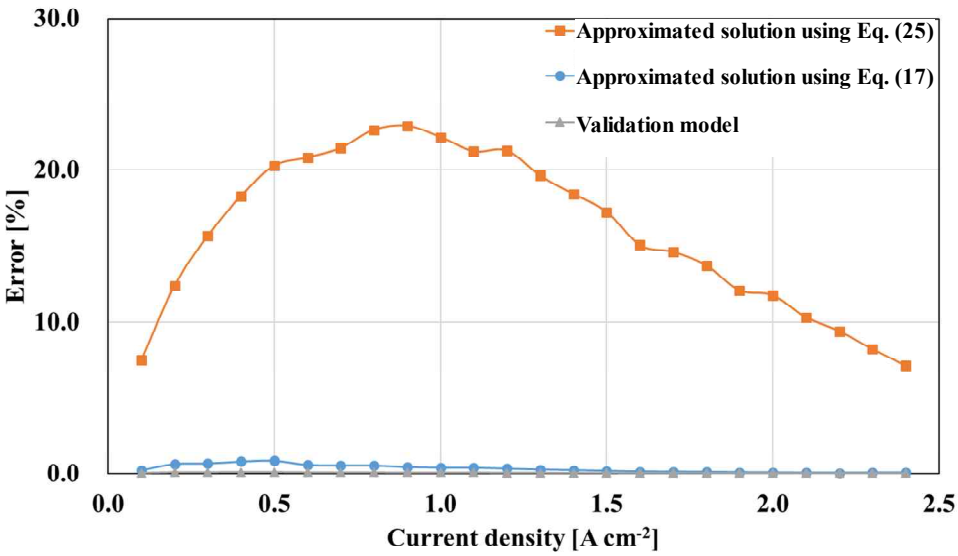

Figure 4.3 Error of the total resistance at RH 100% under H_2/air. Square symbol is the approximated solution using Eq. (26). Circle symbol is the approximated solution using Eq. (18). Triangle symbol is the validation model [1].

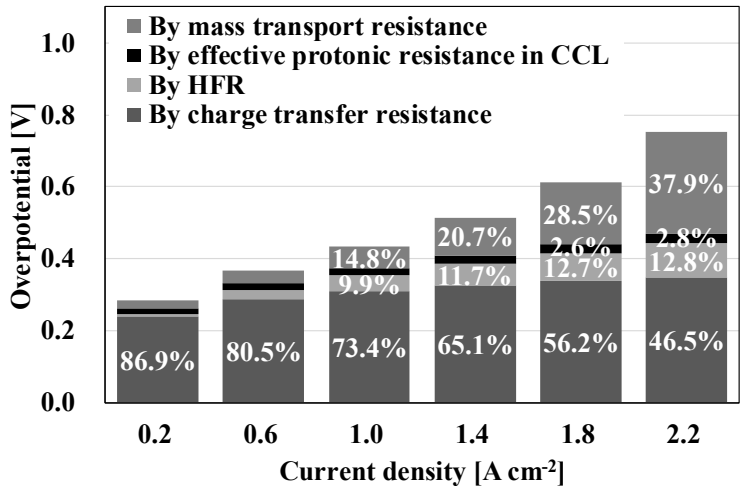

(a)

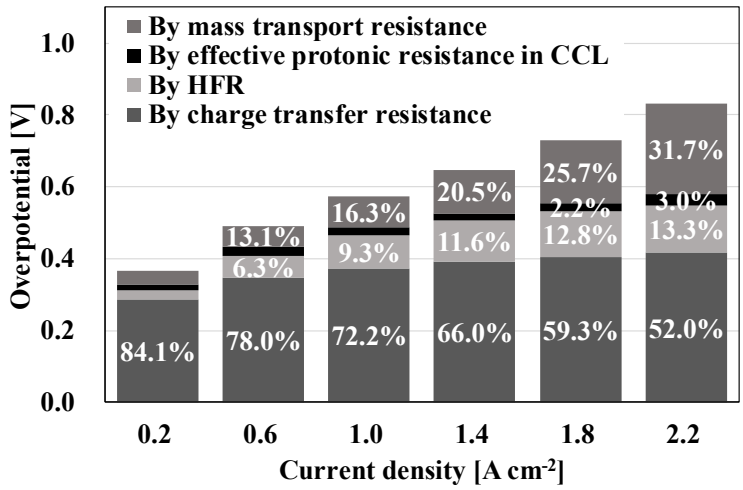

(b)

Figure 4.4 The contribution of the resistances of overpotential in a PEM fuel cell at (a) RH 100%, (b) RH 80% under H_2/air.

Chapter 5. Conclusion

Resistance separation was investigated by EIS and polarization curve. To analyze the EIS, a general solution based on a recursion formula was derived and validated. The solution was simplified using three assumptions; thus, R_{total} can be divided into R_{ct}, HFR, R_P^{eff}, and R_{mass}. When the approximation of $r_p/(r_{ct} + z_W)$ or the assumption on the homogeneity of r_{ct} was not valid, the resistance separation was carried out by EIS and polarization curve. The HFR was estimated from the EIS. The R_{ct}, and R_{mass} were estimated using a polarization curve with the semi-empirical equation. In this case, the equation was identified by the EIS fitting data in the other current density region that satisfied the assumptions. Therefore, R_P^{eff} was calculated using other resistances from the polarization curve and EIS.

The experimental results of R_{ohmic} suggested that HFR and R_P^{eff} are sensitive to the water content. Consequently, as compared with HFR, R_P^{eff} was more strongly dependent on the operating current density and RH condition due to the water content. In addition, R_P^{eff} was smaller than HFR because of the smaller material thickness and the change in the mean distance of ionic transport. To identify the effect of the movement differential, H_2/Heliox experiments were conducted. As a consequence, R_P^{eff} and R_{mass} were changed due to the diffusion effect. The R_P^{eff} was changed under H_2/Heliox, especially in the high current densities because the diffusion coefficient was low under H_2/air.

The $R_P^{eff} \approx R_p/3$ was also derived from the general solution, but this approximation had a relatively large error, more than 5.8% under RH 80% and 7.1% under RH 100%, in this experimental condition.

The overpotential was calculated based on the results of the resistance separation as mentioned above. As a result, the overpotential by R_{ct} was relatively high. However, the overpotential by the other resistance increased as the current density increased, so a portion of the value decreased.

The resistance separation will be helpful to diagnose PEM fuel cells, and the calculation of the overpotential will be useful to identify the effect of the resistance in terms of voltage.

Bibliography

[1] Cruz-Manzo S, Chen R. A generic electrical circuit for performance analysis of the fuel cell cathode catalyst layer through electrochemical impedance spectroscopy. Journal of Electroanalytical Chemistry. 2013;694:45-55.

[2] Park J, Oh H, Ha T, Lee YI, Min K. A review of the gas diffusion layer in proton exchange membrane fuel cells: Durability and degradation. Applied Energy. 2015;155:866-80.

[3] Wang Y, Chen KS, Mishler J, Cho SC, Adroher XC. A review of polymer electrolyte membrane fuel cells: Technology, applications, and needs on fundamental research. Applied Energy. 2011;88:981-1007.

[4] Brunetto C, Moschetto A, Tina G. PEM fuel cell testing by electrochemical impedance spectroscopy. Electric Power Systems Research. 2009;79:17-26.

[5] Page SC, Anbuky AH, Krumdieck SP, Brouwer J. Test Method and Equivalent Circuit Modeling of a PEM Fuel Cell in a Passive State. IEEE Transactions on Energy Conversion. 2007;22:764-73.

[6] Wu J, Yuan X, Wang H, Blanco M, Martin J, Zhang J. Diagnostic tools in PEM fuel cell research: Part I Electrochemical techniques. International Journal of Hydrogen Energy. 2008;33:1735-46.

[7] Makharia R, Mathias MF, Baker DR. Measurement of Catalyst Layer Electrolyte Resistance in PEFCs Using Electrochemical Impedance Spectroscopy. Journal of The Electrochemical Society. 2005;152:A970-A7.

[8] O'Hayre R, Cha SW, Colella W, Prinz FB. Fuel cell fundamentals. Third edition ed: John Wiley & Sons; 2016.

[9] Neyerlin KC, Gu W, Jorne J, Clark A, Gasteiger HA. Cathode catalyst utilizationfor the ORR in a PEMFC - analytical model and experimental validation. Journal of The Electrochemical Society. 2007;154:B279-B87.

[10] Yuan X-Z, Wang H, Colinsun J, Zhang J. AC impedance technique in PEM fuel cell diagnosis—A review. International Journal of Hydrogen Energy. 2007;32:4365-80.

[11] Rezaei Niya SM, Hoorfar M. Study of proton exchange membrane fuel cells using electrochemical impedance spectroscopy technique – A review. Journal of Power Sources. 2013;240:281-93.

[12] Asghari S, Mokmeli A, Samavati M. Study of PEM fuel cell performance by electrochemical impedance spectroscopy. International Journal of Hydrogen Energy. 2010;35:9283-90.

[13] Malevich D, Halliop E, Peppley BA, Pharoah JG, Karan K. Investigation of Charge-Transfer and Mass-Transport Resistances in PEMFCs with Microporous Layer Using Electrochemical Impedance Spectroscopy. Journal of The Electrochemical Society. 2009;156:B216-B24.

[14] van der Merwe J, Uren K, van Schoor G, Bessarabov D. Characterisation tools development for PEM electrolysers. International Journal of Hydrogen Energy. 2014;39:14212-21.

[15] Yoo HD, Jang JH, Ka BH, Rhee CK, Oh SM. Impedance analysis for hydrogen adsorption pseudocapacitance and electrochemically active surface area of Pt electrode. Langmuir. 2009;25:11947-54.

[16] Springer TE, Raistrick ID. Electrical Impedance of a Pore Wall for the FloodedAgglomerate Model of Porous Gas-Diffusion Electrodes. Journal of the Electrochemical Society. 1989;136:1594-603.

[17] Lefebvre MC, Martin RB, Pickup PG. Characterization of Ionic Conductivity Profiles within Proton Exchange Membrane Fuel Cell Gas Diffusion Electrodes by Impedance Spectroscopy. Electrochemical and Solid-State Letters. 1999;2:259-61.

[18] Eikerling M, Kornyshev AA. Electrochemical impedance of the cathode catalyst layer in polymer electrolyte fuel cells. Journal of Electroanalytical Chemistry. 1999;475:107-23.

[19] Freire TJP, Gonzalez ER. Effect of membrane characteristics and humidification conditions on the impedance response of polymer electrolyte fuel cells. Journal of Electroanalytical Chemistry. 2001;503:57-68.

[20] Vielstich W, Gasteiger HA, Lamm A, Yokokawa H. Handbook of Fuel Cells, Fundamentals, Technology and applications: John Wiley & Sons, Ltd; 2010.

[21] Gaumont T, Maranzana G, Lottin O, Dillet J, Guétaz L, Pauchet J. In Operando and Local Estimation of the Effective Humidity of PEMFC Electrodes and Membranes. Journal of The Electrochemical Society. 2017;164:F1535-F42.

[22] Liu Y, Murphy MW, Baker DR, Gu W, Ji C, Jorne J, et al. Proton Conduction and Oxygen Reduction Kinetics in PEM Fuel Cell Cathodes: Effects of Ionomer-to-Carbon Ratio and Relative Humidity. Journal of The Electrochemical Society. 2009;156:B970-B80.

[23] Lange KJ, Sui P-C, Djilali N. Pore scale modeling of a proton exchange membrane fuel cell catalyst layer: Effects of water vapor and temperature. Journal of Power Sources. 2011;196:3195-203.

[24] Kim J-R, Yi JS, Song T-W. Investigation of degradation mechanisms of a high-temperature polymer-electrolyte-membrane fuel cell stack by electrochemical impedance spectroscopy. Journal of Power Sources. 2012;220:54-64.

[25] Kulikovsky AA. Can We Quantify Oxygen Transport in the Nafion Film Covering an Agglomerate of Pt/C Particles? Journal of The Electrochemical Society. 2017;164:F379-F86.

[26] Jaouen F, Lindbergh G. Transient Techniques for Investigating Mass-Transport Limitations in Gas Diffusion Electrodes I. Modeling the PEFC Cathode. Journal of The Electrochemical Society. 2003;150:A1699-A710.

[27] Malevich D, Jayasankar BR, Halliop E, Pharoah JG, Peppley BA, Karan K. On the Determination of PEM Fuel Cell Catalyst Layer Resistance from Impedance Measurement in H2/N2Cells. Journal of The Electrochemical Society. 2012;159:F888-F95.

[28] Gerteisen D. Impact of inhomogeneous catalyst layer properties on impedance spectra of polymer electrolyte membrane fuel cells. Journal of The Electrochemical Society. 2015;162:F1431-F8.

[29] Cruz-Manzo S, Chen R, Greenwood P. An impedance model for analysis of EIS of polymer electrolyte fuel cells under hydrogen peroxide formation in the cathode. Journal of Electroanalytical Chemistry. 2015;745:28-36.

[30] Mann RF, Amphlett JC, Hooper MAI, Jensen HM, Peppley BA, Roberge PR. Development and application of a generalised steady-state electrochemical model for a PEM fuel cell. Journal of Power Sources. 2000;86:173-80.

[31] Cooper KR, Smith M. Electrical test methods for on-line fuel cell ohmic resistance measurement. Journal of Power Sources. 2006;160:1088-95.

[32] Andreaus B. Proton-conducting polymer membranes in fuel cells—humidification aspects. Solid State Ionics. 2004;168:311-20.

[33] Xu H, Song Y, Knuz HR, Fenton JM. Effect of Elevated Temperature and Reduced Relative Humidity on ORR Kinetics for PEM Fuel Cells. Journal of The

Electrochemical Society. 2005;152:A1828-A36.

[34] Iden H, Ohma A, Shinohara K. Analysis of Proton Transport in Pseudo Catalyst Layers. Journal of The Electrochemical Society. 2009;156:B1078-B84.

[35] Zhang J, Tang Y, Song C, Xia Z, Li H, Wang H, et al. PEM fuel cell relative humidity (RH) and its effect on performance at high temperatures. Electrochimica Acta. 2008;53:5315-21.

[36] Modestov AD, Kapustin AV, Avakov VB, Landgraf IK, Tarasevich MR. Cathode catalyst layers with ionomer to carbon mass ratios in the range 0–2 studied by electrochemical impedance spectroscopy, cyclic voltammetry, and performance measurements. Journal of Power Sources. 2014;272:735-42.

[37] Beuscher U, Cleghorn SJC, Johnson WB. Challenges for PEM fuel cell membranes. International Journal of Energy Research. 2005;29:1103-12.

[38] Zhang G, Jiao K, Wang R. Three-Dimensional Simulation of Water Management for High-Performance Proton Exchange Membrane Fuel Cell. SAE International Journal of Alternative Powertrains. 2018;7:233-47.

[39] Rakhshanpouri S, Rowshanzamir S. Water transport through a PEM (proton exchange membrane) fuel cell in a seven-layer model. Energy. 2013;50:220-31.

[40] Guo Q, White RE. A Steady-State Impedance Model for a PEMFC Cathode. Journal of The Electrochemical Society. 2004;151:E133-E49.

[41] Wagner N. Characterization of membrane electrode assemblies in polymer electrolyte fuel cells using a.c. impedance spectroscopy. Journal of Applied Electrochemistry. 2002;32:859-63.

[42] Tang Y, Zhang J, Song C, Liu H, Zhang J, Wang H, et al. Temperature Dependent Performance and In Situ AC Impedance of High-Temperature Using the

Nafion-112 Membrane. Journal of the electrochemical society. 2006;153:A2036-A43.

[43] Eikerling M, Kornyshev AA. Modelling the performance of the cathode catalyst layer of polymer electrolyte fuel cells>. Journal of Electroanalytical Chemistry. 1998;453:89-106.

[44] Kim J, Lee S, Srinivasan S. Modeling of Proton Exchange Membrane Fuel Cell Performance with an Empirical Equation. Journal of The Electrochemical Society. 1995;142:2670-4.

[45] Jaouen F, Lindbergh G, Wiezell K. Transient Techniques for Investigating Mass-Transport Limitations in Gas Diffusion Electrodes II. Experimental Characterization of the PEFC Cathode. Journal of The Electrochemical Society. 2003;150:A1711-A7.

[46] Dotelli G, Omati L, Stampino PG, Brivio D, Grassini P. Effect of Micro Porous Layer (MPL) on Water Management Investigated by Electrochemical Impedance Spectroscopy (EIS) on a Running PEM-FC. ECS Transactions. 2010;33:1115-22.

[47] Cappadonia M, Erning JW, Niaki SMS, Stimming U. Conductance of Nafion 117 membranes as a function of temperature and water content. Solid State Ionics. 1995;77:65-9.

[48] Uosaki K, Okazaki K, Kita H. Conductivity of Nation membranes at low temperatures. Journal of Electroanalytical Chemistry and Interfacial Electrochemistry. 1990;287:163-9.

국 문 초 록

고분자전해질 (PEM) 연료전지 내에서 발생하는 저항의 분리는 연료전지의 효율 및 성능을 향상 시키기 위한 핵심적인 사안이다. 고분자전해질 연료전지의 저항을 분리하기 위해서는 보통 전기화학 임피던스 분광법 (EIS: electrochemical impedance spectroscopy) 과 분극곡선 실험 방법이 많이 사용된다. 이 과정에서, 전기화학 임피던스 분광법의 분석 과정에서 등가회로 선택이 필요하기에, 이에 대한 연구 역시 많이 언급되는 사안이다. 저항의 분리에 대해 연구가 계속 되었으나 촉매층 내 실효 양성자 이동 저항 (effective protonic resistance in cathode catalyst layer) 을 포함한 저항의 분리에 대한 연구는 부족한다. 따라서 본 연구에서는, 분극 곡선과 전기화학 임피던스 분광법을 이용한 고분자 전해질 연료전지 내에서 발생하는 저항을 분리하는 몇 가지 방법을 제안하였다. 이를 전류 밀도와 가습 조건에 따라 수행하였으며, 이를 통해 과전압 (overpotential) 을 계산하여, 각 저항이 성능에 미치는 영향을 전압의 관점에서 분석하였다.

우선 등가회로와 점화식을 이용하여 일반해를 유도하였고, 이를 통해 전기화학 임피던스 분광법의 결과인 Nyquist plot 에 대응시켰다. 이후 전체 저항을 저항으로 나누기 위하여, 전송 선로 모델 내의 분산된 저항을 근사해를 사용하여 분극 곡선의 저항에 대응시켰다. 근사해를 통해 구한 전체 저항의 오차는 상대습도 80, 100% 에서 각각 1.5, 1% 안팎의 오차를 가졌다.

이 분석 방법을 바탕으로 저항과 과전압의 분석이 진행되었다. 막 저항 대비 수분 함유량의 변화에 따른 촉매층 내 실효 양성자 이동 저항이 더 크게 변함을 확인하였다. 본 결과와 관련하여, 헬륨을 이용해 산소의 확산을 달리하여 실험을 수행하였고, 이를 통해 산소 분자의 이동 거리가 달라짐에 따라 촉매층 내 실효 양성자 이동 저항이 낮아짐을 확인하였다. 한편 과전압을 통한 분석에서 전하 이동 저항에 따른 과전압이 가장 컸음을 (46.5 ~ 86.9%) 확인하였고, 옴 저항에 따른 과전압이 전류 밀도에 따라 선형적으로 증가함을 확인했다.

본 연구는, 고분자전해질 연료전지에서 발생하는 저항을 분리 및 분석하였다. 저항 분리를 위해 전기화학 임피던스 분광법과 분극 곡선이 사용되었으며, 이를 통해 두 가지 방법을 제시하였다. 결과적으로, 저항 이동 저항, 고주파 저항, 촉매층 내 실효 양성자 이동 저항, 물질 이동 저항으로 나누었으며, 이를 바탕으로 과전압 관점에서의 전압 손실도 확인했다. 저항 및 과전압의 분석에 대한 본 연구는, 고분자전해질 연료전지의 성능 개성을 위한 연구에 도움이 될 것이다.

주요어: 저항 분리, 과전압, 전기화학 임피던스 분광법, 분극 곡선, 양성자 저항, 수분 함유량

학번: 2017-22150